Investigation of protic ionic liquid electrolytes for porous RuO2 micro-supercapacitors

Jensheer Shamsudeen Seenath, David Pech, Dominic Rochefort

Investigation of protic ionic liquid electrolytes for porous RuO_2 micro-supercapacitors

Jensheer Shamsudeen Seenath[a,b], David Pech[a,*], Dominic Rochefort[b,*]

[a] LAAS-CNRS, Université de Toulouse, CNRS, Toulouse 31400, France.

[b] Département de chimie, Université de Montréal, Montréal, Québec H3C 3J7, Canada.

[*] Corresponding authors: dpech@laas.fr, dominic.rochefort@umontreal.ca

The rapid advancement of the Internet of things (IoT) with applications across various sectors urges the development of miniaturized energy-storage devices that can harvest or deliver energy with high power capabilities. While micro-supercapacitors can meet the high-power requirements of ubiquitous sensors connected to IoT networks, their low voltage and low energy density remain a major bottleneck preventing their wide-scale adoption. In this report, we develop micro-supercapacitors using RuO_2 electrodes providing pseudocapacitive charge storage in protic ionic liquid-based non-aqueous electrolytes while enlarging their operational voltage. The triethylammonium bis(trifluoromethanesulfonyl)imide (TEAH-TFSI)-based interdigitated porous RuO_2 micro-supercapacitors showed an extended cell voltage up to 2 V with 4 times more energy density compared with conventional H_2SO_4 electrolyte. We then developed an all-solid-state micro-supercapacitor using TEAH-TFSI-based ionogel electrolyte able to deliver high areal capacitance (78 mF cm^{-2} at 2 mV s^{-1}) and long-term cycling stability that is superior to state-of-the-art ionogel-based micro-supercapacitors employing carbon-based or pseudocapacitive materials. This study gives a new perspective to develop all-solid-state micro-supercapacitors using pseudocapacitive active materials that can operate in ionic-liquid-based non-aqueous electrolytes compatible with on-chip IoT-based device applications seeking high areal energy/ power performance.

Keywords: RuO_2, Protic Ionic Liquids, Porous Micro-supercapacitor, Ionogel, Pseudocapacitance

1. Introduction

The rising growth of smart and autonomous microelectronic devices in the IoT (Internet of Things) era pushes for the development of advanced microscale energy sources with tailor-made features and customized energy/power requirements [1, 2]. Micro-supercapacitors (MSCs) emerged as potential energy storage devices complementing microbatteries to power ubiquitous sensor networks needed to foster the development of IoT [3]. Due to the fast surface-confined reactions involved in double-layer or pseudocapacitive charging, MSCs show high-power delivery performance through fast charge/discharge along with excellent cycling stability [4-8]. However, these reactions provide low energy density which prevents their large-scale adoptability in real device applications. To mitigate this issue, several studies have been devoted to the engineering of MSC electrode materials and structural architecting of current collectors to enhance the surface area and areal energy density by considering the limited available footprint area [9, 10]. These approaches nonetheless have associated challenges such as complex synthesis routes, maintaining electronic conductivity and mechanical stability, and electrode-electrolyte compatibility issues, among others. Although increasing the active material loading has been a long-standing strategy to improve areal capacitance and the areal energy density, it comes at the expense of higher electrode thickness. Further, it will have a detrimental effect on the robustness of the electrode and lead to poor interfacial and mechanical stability with the current collectors [11, 12]. Another important challenge to solve for reaching high energy density values in MSCs is the limited electrochemical stability window (ESW) as energy stored is directly related to the square of the cell voltage. The electrolytes play a major role in deciding the ESW and liquid-state electrolytes currently employed are troublesome for microfabrication. Therefore, developing novel electrolytes alternative to commonly used aqueous electrolytes compatible with the electrode materials able to afford a wide ESW and feasible incorporation into the commercial microfabrication process requires prompt scientific attention [13-15].

Considering the choice of electrode materials, pseudocapacitive active materials such as metal oxides offer higher specific capacitance than electrochemical double-layer capacitor (EDLC) materials owing to surface controlled redox reactions that makes the major contribution to the charge storage. Among metal oxides, hydrous ruthenium dioxide is known to be the state-of-the-art pseudocapacitive material having the key merits of excellent conductivity, high electrochemical reversibility, and cycling stability [11, 16, 17]. Despite these key characteristics, the high cost prevents their implementation in bulk supercapacitors. On the other hand, micro-supercapacitors (MSCs) require negligible mass loading to meet practical

charge storage performance so their cost is not a limiting factor to their application in MSCs [18]. All of the reports on RuO_2-based MSCs use aqueous electrolytes having narrow ESW ascribed to the inherent limitation of water thermodynamic decomposition potential leading to poor energy density performance. In addition, the use of water as solvent faces the issue of evaporation in real applications considering the small volume of the electrolytes used in MSCs. Finding an alternative to aqueous electrolytes is challenging because protic electrolytes with the accessibility of free H^+ ions are imperative to promote the surface redox reactions in RuO_2 electrodes. Interestingly, protic ionic liquids, a subclass of ionic liquids is a potential non-aqueous electrolyte alternative able to exchange H^+ with RuO_2, hence promoting surface redox reactions while affording a wider ESW [19]. Rochefort *et al.* first successfully demonstrated the origin of pseudocapacitance in RuO_2 using PILs and the capacitance reported is comparable to the aqueous electrolyte [20]. Lindberg *et al.* recently showed that proton availability influences the electrochemical response in MnO_2 electrode, where only the acidic proton of PILs can induce reversible redox reactions while protons attached to aprotic ionic liquids (AILs), e.g., in hydroxy groups fail to bring about any faradaic contribution [21]. Recent reports are suggesting that PILs can be also used in combination with conducting polymers and transition metal nitride-based electrodes [22, 23]. It is known that compared to aqueous electrolytes, PILs display higher viscosity with slower H^+ transfer and it remains to be determined if this is a limiting issue in MSCs. Moreover, as they share the same properties as aprotic ILs, PILs can help to overcome other major challenges associated with currently used electrolytes such as evaporation and encapsulation issues of aqueous-based and flammability of common organic electrolytes [24, 25].

Herein, for the first time, we have developed interdigitated RuO_2 MSCs using novel PIL-based electrolytes able to provide pseudocapacitance with higher ESWs as compared to conventional aqueous electrolytes. The slow proton transport kinetics of PILs were addressed by the inclusion of silicotungstic acid (SiWa, $H_4SiW_{12}O_{40}$) with the PIL composition, which further boosted the pseudocapacitive current response. The porous RuO_2 MSC using SiWa-doped TEAH/TFSI electrolyte manifested a cell voltage exceeding 2 V with an areal capacitance value as high as 86 mF cm^{-2} at 5 mV s^{-1}, which is on par with the performance of porous MSC tested using 0.5 M H_2SO_4 (cell voltage of 0.9 V and areal capacitance of 85 mF cm^{-2} at 5 mV s^{-1}) with a similar number of RuO_2 deposition cycles. The higher cell voltage provides an enhancement of the areal energy density by delivering a value of 31.8 µWh cm^{-2} (*i.e.* 114 mJ cm^{-2}) at 0.5 mW cm^{-2} that can still retain at 11.1 µWh cm^{-2} at a higher power density of 8 mW cm^{-2}. To address issues pertaining to the use of liquid electrolytes in MSCs, an ionogel

composed of poly(vinylidene fluoride) (PVDF) and SiWa-doped TEAH/TFSI (90 wt%) is developed. The ionogel-based all-solid-state MSC showed an areal capacitance of 79 mF cm^{-2} at 2 mV s^{-1} with better long-term cycling capability superior to many of the state-of-the-art all-solid-state micro-supercapacitors employing carbon-based or pseudocapacitive materials [26-33]. The present study vividly represents the feasibility of the direct incorporation of PIL-based RuO_2 MSCs for real IoT-based applications.

2. Materials and methods

2.1. Electrode fabrication

A Ti(100 nm)/Au(300 nm) thin layer was first patterned onto an oxidized silicon wafer using conventional photolithography and lift-off techniques and was electrochemically pretreated by cycling between -0.3 and +1.7 V versus saturated calomel electrode (SCE) in 1 M H_2SO_4 at a scan rate of 100 mV s^{-1} until a stable voltammogram was obtained. The typical dimensions of the interdigitated electrodes are provided in Scheme S1. The total geometrical active surface area of the electrodes is 0.25 cm^2. Porous interdigitated metallic current collectors were selectively electrodeposited using the dynamic hydrogen bubble template (DHBT) technique onto conductive areas (bath solution contains 2 x 10^{-3} M of $HAuCl_4.3H_2O$ in 3 M H_2SO_4 and the applied current density was 5 A cm^{-2} for 10 min with Pt mesh as counter electrode and SCE as reference electrode). The porous substrate was rinsed with deionized water before ruthenium oxide (RuO_2) deposition. Electrodeposition of hydrous RuO_2 onto the interdigitated porous Au was done by cycling the electrodes between -0.3 and +0.95 V versus SCE at 50 mV s^{-1} for 300 cycles in a solution of 0.01 M $RuCl_3.xH_2O$ in 0.2 M KCl-HCl buffer medium. The electrode was then annealed at 150 °C for 1 h.

2.2. Protic Ionic Liquids (PILs) synthesis

All the PILs were prepared by the slow addition of the equimolar amount of acid into each respective base while stirring in an ice bath. To prevent trace amounts of water from the precursor or atmosphere, the mixtures were heated at 60 °C for 24 h under vacuum. The vials containing PIL samples were sealed and kept in the glove box under argon for the measurements. Water content was measured using Karl Fisher titration.

2.3. Preparation of ionogel

Ionogel was produced by mixing a poly(vinylidene fluoride) ($M_w \approx 534{,}000$, Sigma Aldrich) in acetone and stirred until a uniform viscous solution is formed. After, SiWa ($H_4SiW_{12}O_{40}$)

doped TEAH-TFSI electrolyte (90 wt%) was added to this solution and stirred for 2 h. The all-solid-state micro-supercapacitor was realized by carefully drop-casting the ionogel electrolyte onto the interdigitated RuO_2 electrode and letting it dry at room temperature.

2.4. Material Characterizations

The electrochemical characterizations were performed with an SP-240 BioLogic potentiostat. The surface morphology of the electrodes was examined by scanning electron microscopy (SEM) on a Hitachi S-4800 field emission electron microscope. The surface chemical composition of ruthenium oxide was estimated via X-ray photoelectron spectroscopy (XPS) using a Thermo Scientific spectrometer operating with a monochromatic Al Kα X-ray source (1486.6 eV). The density and viscosity measurements of PILs were conducted simultaneously with an Anton-Paar DMA 5000 M and Lovis 2000ME, which use an oscillating U-tube principle for density and a rolling ball (falling sphere method) viscometer. The ionic conductivity was measured with a Jenway microvolume 120 mm reach glass conductivity probe (model 027815), made of two platinized platinum plates.

3. Results and Discussion

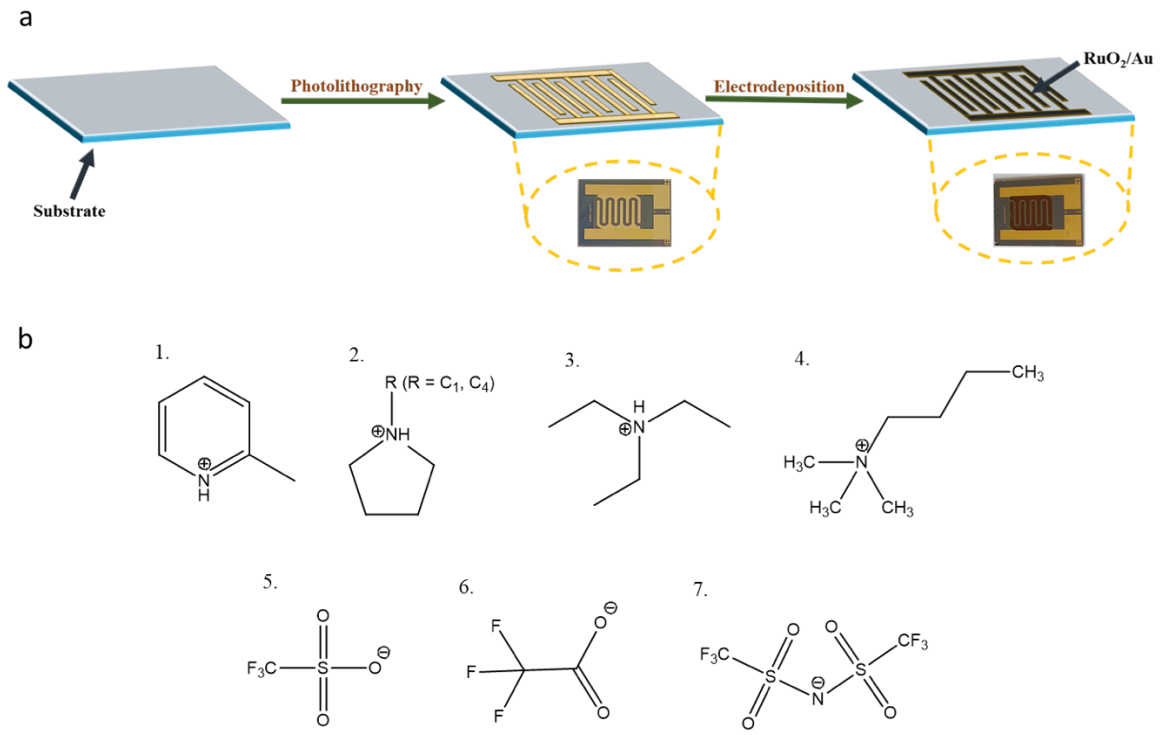

Scheme 1. *a. Schematic of realising interdigitated Au substrates and the deposition of RuO_2 with photographs of the device; b. Structures of the cation and anion groups of ionic liquid candidates explored for RuO_2 MSCs (1. 2-MePy = 2-methyl pyridinium, 2. Pyr_{1H} = 1-methyl*

pyrrolidinium, Pyr_{4H} = 1-butyl pyrrolidinium, 3. TEAH = triethylammonium, 4. BTMA = butyl-trimethyl ammonium, 5. Tf = trifluromethanesulfonate, 6. TFA = trifluoroacetate acid, 7. TFSI = bis(trifluoromethanesulfonyl)imide).

The initial objective was to figure out the electrochemical stability window of RuO_2 electrodes in various protic ionic liquids (PILs). For this, we first deposited hydrous ruthenium oxide electrochemically on interdigitated flat Au substrates (**Scheme 1a**), the deposition method was presented in our earlier reports [18]. The successful deposition of the active material has been confirmed using scanning electron microscopy (SEM) and Energy-dispersive X-ray spectroscopy (EDS) elemental mapping (**Fig. S1)**. It is noteworthy that the electrodeposition technique is a viable and scalable route concerning the commercial microfabrication process. The structure of the PILs investigated in our current study on RuO_2 MSCs is shown in **Scheme 1b**. The choice of these electrolyte candidates is based on their physicochemical properties with a range of commonly available structures that are easier to synthesis and remain stable under normal operational conditions [34-37]. It is important to mention that few of these selected structures of PILs are already reported for conventional supercapacitors using metal-oxide electrodes or their aprotic analogues are used for EDLC-based electrodes [20, 38-42]. The key properties of PILs that are desirable for energy storage include high ionicity (large Δ pKa between the constituents), high ionic conductivity/lower viscosity, and wide stability windows. For instance, while pyrrolidinium or alkyl ammonium-based PILs can provide a wide stability window, the PIL composed of pyridine-based cation and trifluoroacetic acid anion can render high ionicity due to their large pKa difference [35, 38, 41, 43].

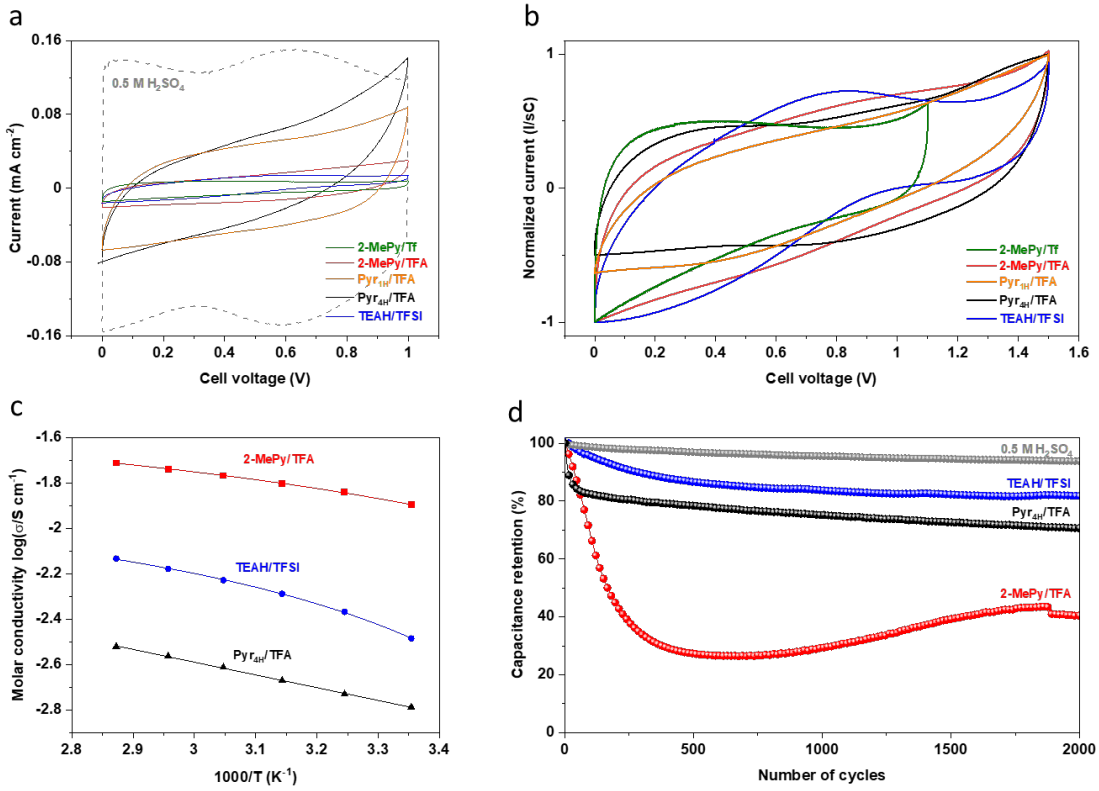

Fig. 1. *a. Cyclic voltammetry (CV) curves of RuO_2 on interdigitated flat Au substrates tested in different PILs and their comparison with 0.5 M H_2SO_4 (scan rate of 100 mV s^{-1}); b. Normalised CVs of RuO_2 in PILs at a scan rate of 100 mV s^{-1}; c. Arrhenius plots for the PILs with measurements done at an interval of 10°C from 25 to 75°C; d. Cycling stability performance of RuO_2 MSCs in different electrolytes at 1 mA cm^{-2}.*

Our next goal was to determine the electrochemical window of RuO_2 MSC in these electrolytes. To achieve this, we run cyclic voltammetry (CV) scanning starting at open circuit potential to a point where irreversibility due to electrolyte oxidation and electrode damage become conspicuous. To have a better differentiation with the standard 0.5 M H_2SO_4 electrolyte, a comparison of the CVs of RuO_2 MSCs between 0 and 1 V using different PILs as well as in the aqueous electrolyte is shown in **Fig. 1a**. Although a higher current density is achieved with the aqueous acidic electrolyte due to faster redox kinetics and efficient utilization of active sites, the ESW is limited to *ca.* 1 V owing to the thermodynamic decomposition limit of water. It should be noted that among the synthesized PILs, 2-MePy/Tf and Pyr_{1H}/TFA remained in the solid or semi-solid form, therefore it is required to use an organic solvent and aprotic ionic-liquid medium for the dilution and to use as electrolyte for the electrochemical characterisation. **Fig. 1b** shows the normalized CVs (the current, *I*, has been normalized by the scan rate, *s*, and capacitance, *C*) of RuO_2 MSCs tested using PILs at their maximum cell

voltage (1.1 V for 2-MePy/Tf and 1.5 V for the rest of the PILs (2-MePy/TFA, Pyr_{1H}/TFA, Pyr_{4H}/TFA, and TEAH/TFSI)). The CV curves showed pseudo rectangular shapes showing the pseudocapacitive charge transfer between PIL and RuO_2 beyond the thermodynamic stability window of conventional aqueous electrolytes. In order to provide a comparison of the impact of the maximum voltage across the electrolytes used, the CV curve of RuO_2 MSC using 0.5 M H_2SO_4 up to 1.5 V is shown in **Fig. S5.** A large current onset at 1.1 V which corresponds to the irreversible oxidation of water. To evaluate how the conductivity affects the electrochemical response of the MSC, the temperature dependence of molar conductivity is represented using the Arrhenius plot (**Fig. 1c)**. The conductivity strongly depends on the ion-ion interaction and in PILs, hydrogen bonding also plays a role in the intermolecular interactions [44]. The Pyr_{4H}/TFA showed an ideal fit in the Arrhenius plot at all temperatures, which we believe could stem from the higher water content (>1000 ppm) as it can disrupt the strong ion interactions in the PIL. On the other hand, both TEAH/TFSI and 2-MePy/TFA showed curvature deviation at lower temperatures. For such systems, the Vogel–Tamman–Fulcher (VTF) fit is used to describe the ion conduction behaviour, which implies the increase in temperature is not entirely resulting in increased ion mobility. The Walden plot gives a qualitative analysis of the ionicity of PILs by comparing ionicity and equivalent conductivity values, which help us to understand the proton transfer property of PILs. An ideal line in the Walden plot is obtained based on the measurements using 1 M KCl solution. An ionic liquid of "good" quality lies in proximity to this line and those of poor quality will be lower than this line as described by Angell and co-workers [45]. The data corresponding to 0.5 M H_2SO_4 will appear above the ideal line owing to the Grotthus transport mechanism that is well-known in the literature [46]. The 2-MePy/TFA showed a value exactly on the reference KCl (**Fig. S2)**, indicating a good ionicity, which is in accordance with some of the earlier reports of using 2-MePy/TFA where a large Δ pKa between the constituents granted a higher ionicity and a strong proton transfer without forming a neutral species by volatilization during the heating step [38]. Both TEAH/TFSI and Pyr_{4H}/TFA are positioned slightly below and closer to the ideal line with slight ion pairing in the latter as is expected from PILs, where charge transport occurs via a vehicle-type mechanism. Overall, the conductivity values of investigated PILs occupy the region of good ionic liquids in the Walden plot and are comparable to most of the PILs reported in the literature. Next, we performed cycling of the electrodes in all these electrolytes as long-term cycling is a key requisite for the practical application of MSCs. Despite a higher ionic conductivity, 2-MePy/TFA showed lower cyclability with a sharp capacitance drop up to *ca.* 500 cycles which remained stable afterward (**Fig. 1d)**, this can be ascribed to the significant damage happening to the RuO_2 electrode during

the charge-discharge cycles and the active material dissolution in the electrolyte. The changes in the Ru metallic state after cycling in 2-MePy/TFA were further confirmed using XPS analysis of the electrodes before and after the long cycling **(Fig. S3 & S4b)**, which showed a major reduction in the Ru 3p signal which is ascribed to the clear degradation of the active material, RuO_2. On the other hand, TEAH/TFSI showed better long-term cycling stability with RuO_2, where the Ru 3p signals obtained from XPS remained intact **(Fig. S4a).** Provided the high ionicity, stability window, and long-term cyclability of TEAH/TFSI, we decided to perform further detailed electrochemical studies using this particular PIL.

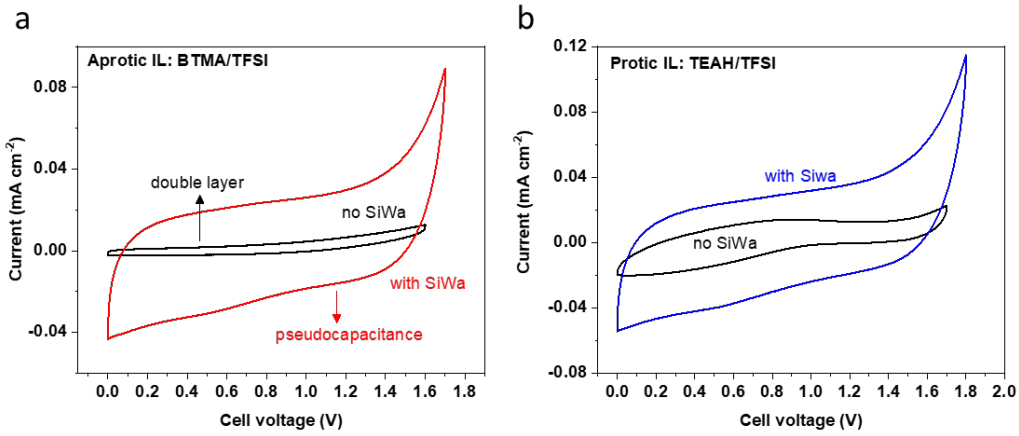

Fig. 2. *Capacitive behaviour of protic and aprotic IL based on TFSI anion for RuO_2 MSCs using flat substrate in ILs with SiWa doping (10 wt%). a. CV curves (100 mV s^{-1}) in an aprotic ionic-liquid, butyl-trimethyl ammonium trifluoromethane sulfonyl imide (BTMA/TFSI) before and after SiWa doping; b. CV curves using TEAH/TFSI before and after SiWa doping.*

Although PILs can exchange protons at the RuO_2 electrode surface, the lack of swift proton (H^+) transportability due to vehicle-type charge transport limits the rate performance [44, 47]. To address this issue, we decided to dope TEAH/TFSI with a solid ionic conductor of H^+, silicotungstic acid, and monitored the change in the current response and voltage window. The SiWa belong to the family of heteropolyacids, which are hydrous salts exhibiting high proton conductivity (e.g. 0.027 S cm^{-1} for $SiWa.28H_2O$) at room temperature owing to hydrogen-bonded conduction pathways in the crystal lattice originate from a large number of crystallized water molecules in the crystal hydrate and the dynamic dissociation of co-crystallized water molecules in the crystal hydrate via interactions with oxygen atoms of the Keggin anion, which increases the density of free protons [48, 49]. In our previous report, we successfully demonstrated the impact of SiWa with an aprotic ionic liquid electrolyte and the

pseudocapacitive current enhancement using $RuO_xN_yS_z$ electrodes [50]. The study of SiWa with PILs have never been done before and it would be interesting to explore the compatibility and electrochemical behavior in comparison to an aprotic ionic liquid of a similar structure as TEAH/TFSI. The CV study revealed a huge enhancement in the pseudocapacitive current response in SiWa-doped butyl-trimethyl ammonium trifluoromethane sulfonyl imide (BTMA/TFSI), the aprotic analogue chosen for the study (**Fig. 2a)**, showing SiWa bestowed freely available H^+ ions to promote the surface redox reactions with RuO_2 which previously only had a double-layer contribution. On the other hand, in TEAH/TFSI, the SiWa accelerated the charge transport as evident from the rise in the current values owing to a combined Grotthus (from SiWa) and vehicle-type (from TEAH/TFSI) transport (**Fig. 2b)**.

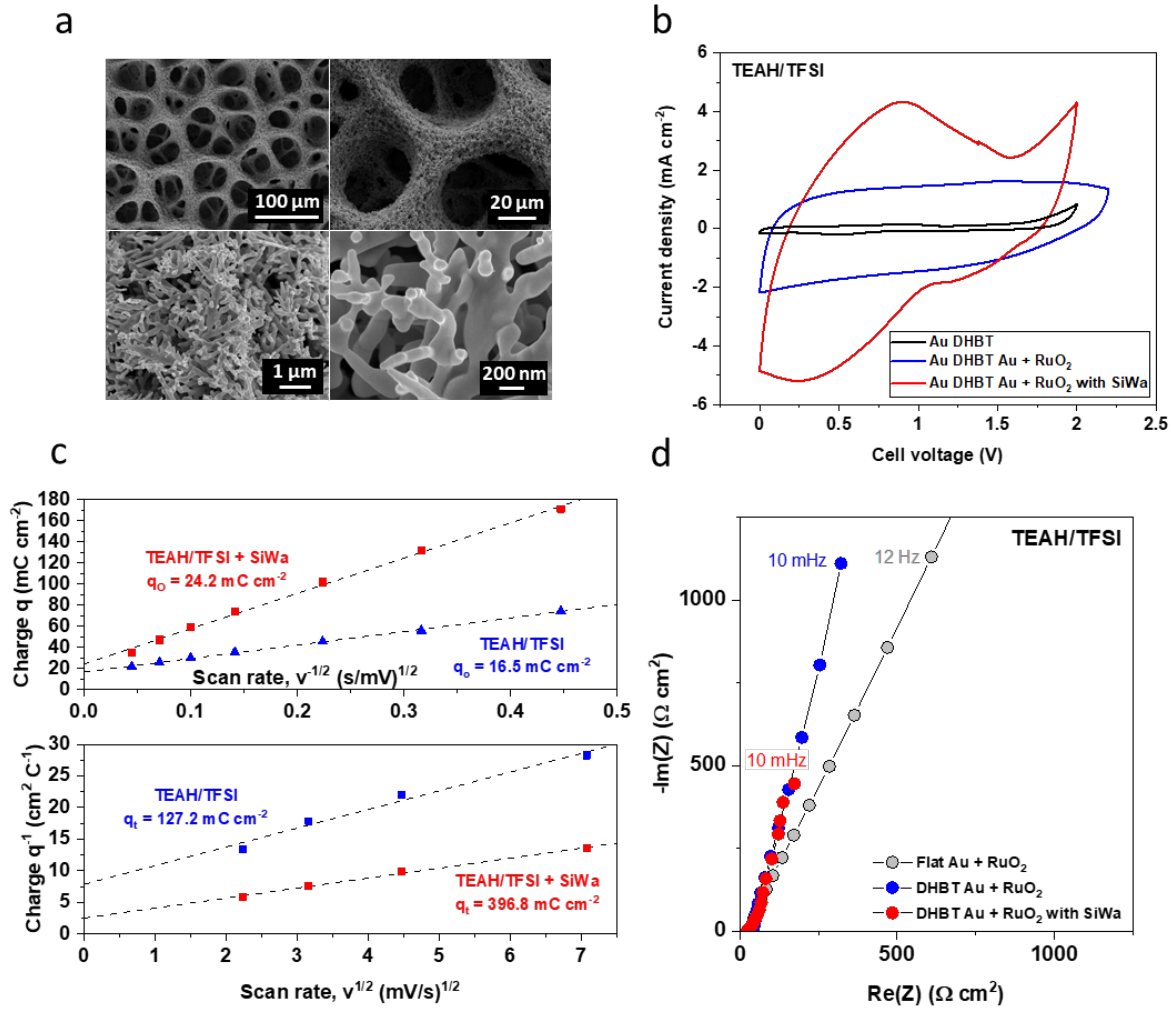

***Fig. 3**. Electrochemical performance RuO_2 MSC using interdigitated porous DHBT Au substrate characterised in neat TEAH/TFSI and SiWa doped TEAH/TFSI; a. Scanning electron microscopy (SEM) images at different magnification of DHBT Au substrate with RuO_2 deposition; b. Comparison of CVs with the bare DHBT Au and after RuO_2 deposition at a scan*

rate of 100 mV s^{-1}; c. Determination of the outer capacitance (C_o) and total capacitance (C_t) of the electrode obtained by calculating the voltammetric charge, q, as a function of the sweep rate, v.; d. Comparison of Nyquist plots of RuO_2 deposited on interdigitated flat Au vs. DHBT Au substrate.*

To demonstrate the practical viability of MSCs, developing high roughness current collectors having high electrochemically active surface area is imperative to increase the active material loading by keeping the limited footprint space available. Similar to our previous reports [11, 18, 50], we prepared high surface area interdigitated Au current collectors through the dynamic hydrogen bubble template (DHBT) method. The typical interconnected highly porous gold current collector containing RuO_2 deposits is revealed from the SEM image **(Fig. 3a).** The thickness of the porous electrodes after the RuO_2 deposition is ca. 20 μm. A comparison of the CV curves of the RuO_2 electrodes tested in TEAH/TFSI and TEAH/TFSI + SiWa electrolytes are shown in **Fig. 3b**. A distinguishable gain in the current density is observed using SiWa doped electrolyte with redox peaks that appeared conspicuous, which reveals proton abundance in the electrolyte and facile transfer of H^+ at the RuO_2, promoting the surface-controlled faradaic process. Importantly, going from flat to high roughness Au substrates showed a higher cell voltage primarily because of a higher resistance coming from DHBT substrates with increased electrode thickness. The CV curves at different scan rates showed reversibility of the redox reactions with a raise in the current upon increase in the scan rate **(Fig. S6a)**. The galvanostatic charge-discharge (GCD) curves at various current densities showed a non-linear shape typical for pseudocapacitive materials with long discharge time **(Fig. S6b)**. It's noteworthy that the charge accessibility of RuO_2 using PILs might behave differently in comparison with aqueous electrolytes on account of their viscous nature in combination with a highly porous substrate and we might have a significant fraction of active material not participating As a testimony to this, we used the method proposed by Trasatti *et al*., by calculating the outer charge (q_o) and total charge (q_t) as it is often used for RuO_2 materials [51] **(Fig. 3c)**. The q_o and q_t analysis of the electrode is done by plotting voltammetric charge q^* as a function of the sweep rate, v. Compared to the results from RuO_2 tested in aqueous 0.5 M H_2SO_4 electrolyte [18], PIL showed a lower q_o contribution (13%), which could be attributed to the larger size of the cations and anions in PILs making it difficult to access the densely connected pores lowering the charge storage kinetics. We strongly believe that this issue can be well addressed in the future with a better understanding of the underlying charge storage mechanism and rational designing of the current collectors offering better charge accessibility and efficient utilization of the active sites. Further, to unveil the change in

electrolyte resistance in different substrates, the Nyquist plots correspond to RuO_2 MSCs tested in the same electrolyte with interdigitated flat *vs.* DHBT Au substrate configurations are acquired and shown in **Fig. 3d**. A low equivalent series resistance (ESR) of *ca.* 23.8 Ω cm^2 is obtained for porous RuO_2 MSC using SiWa-doped TEAH/TFSI with a near-vertical straight line in the low-frequency region indicating an ideal capacitive behaviour. The Bode plot was then used to determine the relaxation time constant (τ_0) that gives an idea about the minimum time required to reach 50 % of the capacitive energy storage, which was calculated from the characteristic frequency corresponding to a phase angle of 45°. The low τ_0 values of 2.6 and 3.9 s. for the neat and SiWa doped TEAH/TFSI, respectively, further corroborated the facilitated ion transport and a higher power delivery performance **(Fig. S7)**.

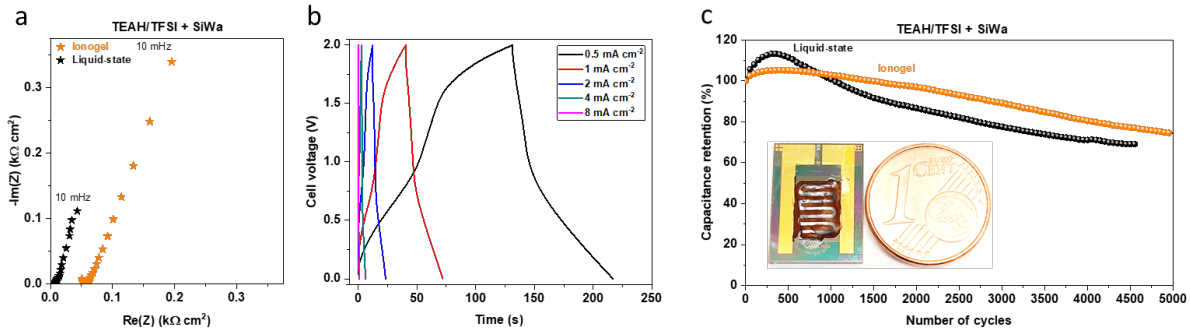

Fig. 4. *Electrochemical performance of porous RuO_2-based all-solid-state MSC. a. Electrochemical impedance spectroscopy (EIS) of MSCs using liquid-state and ionogel TEAH/TFSI electrolyte; b. GCD curves of the all-solid-state MSC at different current densities; c. Long-term cycling stability study using liquid-state and ionogel electrolyte (inset represents a typical porous RuO_2-MSC device with ionogel coating).*

To envision the practical application of MSCs, it is imperative to develop solid-state-electrolyte which are leakage-free and able to perform well under real operational conditions. Since SiWa doped TEAH/TFSI showed the best performance as the electrolyte for porous RuO_2 MSCs, we developed an ionogel using TEAH/TFSI + SiWa in combination with poly(vinylidene fluoride)-based host polymer (details are given in the experimental session). The choice of PVDF is obvious as it is a commonly used host matrix for the preparation of the ionogels in flexible energy storage devices as it offers high mechanical and thermal stability along with a high dielectric constant [52-54]. To better understand the change in the ESR while transitioning from liquid to gel-state of the electrolyte, we rely on the impedance spectroscopy measurement **(Fig. 4a)**. A higher ESR value of 52.5 Ω cm^2 for the solid-state device (more than double as

compared to the liquid-state) can be attributed to the restricted ionic movement and the device being all-solid-state. The pseudo-rectangular-shaped CV curves at different scan rates **(Fig. S8)** showed the reversibility of the redox reactions. The non-linear-looking GCD curves at various current densities indicate pseudocapacitive-based charge storage **(Fig. 4b)**. Compared to the CV and GCD curves of the MSCs using a liquid-state electrolyte, the all-solid-state MSC showed a characteristic resistive signature attributed to their higher ESR value. The solid-state MSC device showed a highest capacitance value of 79 mF cm^{-2} at 2 mV s^{-1}, which is closer to the performance reported using liquid-state electrolyte (86 mF cm^{-2} at 5 mV s^{-1}). The energy *vs.* power density comparison of porous RuO_2 MSCs tested in different electrolytes is represented in a Ragone plot to draw a broader perspective about their key difference in the areal performance matrix which is vital for the practical application of MSCs **(Fig. S10)**. The higher cell voltage of PIL compared to the aqueous 0.5 M H_2SO_4 electrolyte led to an enhanced energy density performance of 31.8 μWh cm^{-2} at 0.5 mW cm^{-2} as compared to the MSC tested using 0.5 M H_2SO_4 (7.6 μWh cm^{-2} at 0.23 mW cm^{-2}). The solid-state MSC exhibited an energy density value of 17.26 μWh cm^{-2} at 0.56 mW cm^{-2}, which was slightly lower as compared to the liquid electrolyte. Table S1 (Supporting Information) shows a comparison of the electrochemical performance of porous RuO_2 MSCs with state-of-the-art in-plane MSCs consisting of carbon-based or pseudocapacitive materials. It's important to note that an explicit comparison with the performance reported in literature makes it difficult as there are big differences in the synthesis route, measurements followed, etc. and our goal here was to show an overview of the areal performance in different states of the electrolyte. In addition, even with pseudocapacitive electrode material and ionic-liquid electrolytes, the MSCs displayed a good long-term cycling performance up to 5000 cycles **(Fig. 4c)**. We did try the electrochemical measurements of the all-solid-state MSC device in the 1.5 V window to understand whether it would lead to an improved electrochemical or cycling performance **(Fig. S9)**. However, lowering the stability window did not lead to an improvement in the cycling performance. Nevertheless, it's worth noting that the performance including areal capacitance, energy density, and cycle life can be greatly improved in the future with a rational choice of the PIL and a better understanding of the underlying charge storage mechanism. Although there's plenty of room open to address these important questions, the performance reported here clearly demonstrates the potential of RuO_2-based all-solid-state MSCs for future IoT-based applications.

4. Conclusion

In summary, we have successfully demonstrated the use of protic ionic liquids as novel electrolytes for micro-supercapacitors employing electrodeposited RuO_2 electrodes. The surface-controlled proton-coupled electron transfer reaction is realised through the transfer of protons (H^+) from the base cation of PIL. The inclusion of SiWa granted the availability of free H^+ ions and enhanced pseudocapacitive current response with enlarged cell voltage. The use of PILs for real device application was further accomplished by the use of RuO_2 deposited on interdigitated porous Au current collectors having a high area enlargement factor (AEF). The resultant porous MSC rendered a cell voltage exceeding 2 V with areal capacitance as high as 86 mF cm^{-2} at 5 mV s^{-1} and superior energy density performance of 31.8 μWh cm^{-2} at 0.5 mW cm^{-2}. The ionogel-based all-solid-state MSC showed the potential integration in real on-chip device applications rendering similar performance as liquid-state electrolyte with superior long-term cycling stability. We are convinced and important to emphasize that the performance can be greatly improved through rational architecting of porous MSC current collectors and conformal loading of the active material in combination with the ideal choice of the PIL. This work opens up new avenues for the development of high-performance MSC devices employing a combination of pseudocapacitive materials and ionic liquid-based safe electrolytes having better encapsulation and higher energy storage performance.

Acknowledgements

The authors acknowledge the support from the European Research Council (ERC, Consolidator Grant, ERC-2017-CoG, Project 771793 3D-CAP) and the financial support of the Natural Science and Engineering Council (NSERC, Project RGPIN-2019-05970). DR and JSS thank the CQMF-QCAM (Quebec Center for Advanced Materials). This work was supported by LAAS-CNRS technology platform, a member of Renatech network.

References

[1] A. Whitmore, A. Agarwal, L. Da Xu, *The Internet of Things—A survey of topics and trends*, **Inf. Syst. Front.**, 17 (2014) 261-274, 10.1007/s10796-014-9489-2

[2] C. Lethien, J. Le Bideau, T. Brousse, *Challenges and prospects of 3D micro-supercapacitors for powering the internet of things*, **Energy Environ. Sci.** 12 (2019) 96-115, 10.1039/c8ee02029a

[3] N.A. Kyerematen, T. Brousse, D. Pech, *Microsupercapacitors as miniaturized energy-storage components for on-chip electronics*, **Nat. Nanotechnol.** 12 (2017) 7-15, 10.1038/nnano.2016.196
[4] V. Augustyn, P. Simon, B. Dunn, *Pseudocapacitive oxide materials for high-rate electrochemical energy storage*, **Energy Environ. Sci.** 7 (2014) 1597-1614, 10.1039/c3ee44164d
[5] M. Beidaghi, Y. Gogotsi, *Capacitive energy storage in micro-scale devices: recent advances in design and fabrication of micro-supercapacitors*, **Energy Environ. Sci.** 7 (2014) 867-884, 10.1039/c3ee43526a
[6] Y. Wang, Y. Song, Y. Xia, *Electrochemical capacitors: mechanism, materials, systems, characterization and applications*, **Chem. Soc. Rev.** 45 (2016) 5925-5950, 10.1039/c5cs00580a
[7] C. Choi, D.S. Ashby, D.M. Butts, R.H. DeBlock, Q. Wei, J. Lau, B. Dunn, *Achieving high energy density and high power density with pseudocapacitive materials*, **Nat. Rev. Mater.** 5 (2019) 5-19, 10.1038/s41578-019-0142-z
[8] L.B. Karroubi, S.G. Patnaik, B.*D. Assresahegn, B. Bounor, C.C.H. Tran, S.H. Choudhury, D. Bourrier, D. Guay, D. Pech, Highly porous scaffolds for Ru-based microsupercapacitor electrodes using hydrogen bubble templated electrodeposition*, **Energy Storage Mater.** (2022), 10.1016/j.ensm.2022.02.009
[9] L. Liu, H.P. Zhao, Y. Lei, *Advances on three-dimensional electrodes for micro-supercapacitors: A mini-review*, **Infomat.** 1 (2019) 74-84, 10.1002/inf2.12007
[10] S.H. Park, G. Goodall, W.S. Kim, *Perspective on 3D-designed micro-supercapacitors*, **Mater Des.** 193 (2020) 108797, 10.1016/j.matdes.2020.108797
[11] A. Ferris, S. Garbarino, D. Guay, D. Pech, *3D RuO(2) Microsupercapacitors with Remarkable Areal Energy*, **Adv. Mater.**, 27 (2015) 6625-6629, 10.1002/adma.201503054
[12] Y.L. Wang, Y. Zhang, J.M. Liu, G.L. Wang, F.Z. Pu, A. Ganesh, C. Tang, X.W. Shi, Y.D. Qiao, Y.Z. Chen, H.G. Liu, C.C. Kong, L. Li, *Boosting areal energy density of 3D printed all-solid-state flexible microsupercapacitors via tailoring graphene composition*, **Energy Storage Mater.** 30 (2020) 412-419, 10.1016/j.ensm.2020.05.034
[13] T. Famprikis, P. Canepa, J.A. Dawson, M.S. Islam, C. Masquelier, *Fundamentals of inorganic solid-state electrolytes for batteries*, **Nat. Mater.** 18 (2019) 1278-1291, 10.1038/s41563-019-0431-3
[14] L. Xia, L.P. Yu, D. Hu, G.Z. Chen, *Electrolytes for electrochemical energy storage*, **Mater. Chem. Front.** 1 (2017) 584-618, 10.1039/c6qm00169f
[15] C. Zhong, Y. Deng, W. Hu, J. Qiao, L. Zhang, J. Zhang, *A review of electrolyte materials and compositions for electrochemical supercapacitors*, **Chem. Soc. Rev**., 44 (2015) 7484-7539, 10.1039/c5cs00303b
[16] D. Galizzioli, F. Tantardini, S. Trasatti, R*uthenium dioxide: a new electrode material. I. Behaviour in acid solutions of inert electrolytes*, **J. Appl. Electrochem.** 4 (1974) 57-67, 10.1007/BF00615906
[17] K. Brousse, S. Pinaud, S. Nguyen, P.F. Fazzini, R. Makarem, C. Josse, Y. Thimont, B. Chaudret, P.L. Taberna, M. Respaud, P. Simon, *Facile and Scalable Preparation of Ruthenium*

Oxide‐Based Flexible Micro‐Supercapacitors, **Adv. Energy Mater**., 10 (2019) 1903136, 10.1002/aenm.201903136
[18] A. Ferris, D. Bourrier, S. Garbarino, D. Guay, D. Pech, 3D *Interdigitated Microsupercapacitors with Record Areal Cell Capacitance*, **Small**, 15 (2019) 1901224, 10.1002/smll.201901224
[19] T. Stettner, A. Balducci, *Protic ionic liquids in energy storage devices: past, present and future perspective*, **Energy Storage Mater.** 40 (2021) 402-414, 10.1016/j.ensm.2021.04.036
[20] D. Rochefort, A.L. Pont, *Pseudocapacitive behaviour of RuO_2 in a proton exchange ionic liquid*, **Electrochem. Commun.** 8 (2006) 1539-1543, j.elecom.2006.06.032
[21] S. Lindberg, S. Jeschke, P. Jankowski, M. Abdelhamid, T. Brousse, J. Le Bideau, P. Johansson, A. Matic, *Charge storage mechanism of α-MnO_2 in protic and aprotic ionic liquid electrolytes*, **J. Power Sources**, 460 (2020) 228111, 10.1016/j.jpowsour.2020.228111
[22] A. Djire, J.Y. Ishimwe, S. Choi, L.T. Thompson, *Enhanced performance for early transition metal nitrides via pseudocapacitance in protic ionic liquid electrolyte*s, **Electrochem. Commun.** 77 (2017) 19-23, 10.1016/j.elecom.2017.02.001
[23] F. Al-Zohbi, J. Jacquemin, F. Ghamouss, B. Schmaltz, M. Abarbri, K. Cherry, M.F. Tabcheh, F. Tran-Van, *Impact of the aqueous pyrrolidinium hydrogen sulfate electrolyte formulation on transport properties and electrochemical performances for polyaniline-based supercapacitor*, **J. Power Sources**, 431 (2019) 162-169, 10.1016/j.jpowsour.2019.05.018
[24] M. Armand, F. Endres, D.R. MacFarlane, H. Ohno, B. Scrosati, *Ionic-liquid materials for the electrochemical challenges of the future*, **Nat. Mater.** 8 (2009) 621-629, 10.1038/nmat2448
[25] J. Le Bideau, L. Viau, A. Vioux, *Ionogels, ionic liquid based hybrid materials*, **Chem. Soc. Rev**., 40 (2011) 907-925, 10.1039/c0cs00059k
[26] J. Feng, X. Sun, C. Wu, L. Peng, C. Lin, S. Hu, J. Yang, Y. Xie, *Metallic few-layered VS_2 ultrathin nanosheets: high two-dimensional conductivity for in-plane supercapacitors*, **J. Am. Chem. Soc**., 133 (2011) 17832-17838, 10.1021/ja207176c
[27] M. Brachet, T. Brousse, J. Le Bideau, *All Solid-State Symmetrical Activated Carbon Electrochemical Double Layer Capacitors Designed with Ionogel Electrolyte*, **ECS Electrochem. Lett.** 3 (2014) A112-A115, 10.1149/2.0051411eel
[28] B. Hsia, J. Marschewski, S. Wang, J.B. In, C. Carraro, D. Poulikakos, C.P. Grigoropoulos, R. Maboudian, *Highly flexible, all solid-state micro-supercapacitors from vertically aligned carbon nanotubes*, **Nanotechnology**, 25 (2014) 055401, 10.1088/0957-4484/25/5/055401
[29] D. Kim, G. Lee, D. Kim, J.S. Ha, *Air-stable, high-performance, flexible microsupercapacitor with patterned ionogel electrolyte*, **ACS Appl. Mater. Interfaces**, 7 (2015) 4608-4615, 10.1021/am5077843
[30] M. Brachet, D. Gaboriau, P. Gentile, S. Fantini, G. Bidan, S. Sadki, T. Brousse, J. Le Bideau, *Solder-reflow resistant solid-state micro-supercapacitors based on ionogels*, **J. Mater. Chem. A**, 4 (2016) 11835-11843, 10.1039/c6ta03142k
[31] S.H. Zheng, J.M. Ma, Z.S. Wu, F. Zhou, Y.B. He, F.Y. Kang, H.M. Cheng, X.H. Bao, *All-solid-state flexible planar lithium ion micro-capacitors*, **Energy Environ. Sci.**, 11 (2018) 2001-2009, 10.1039/c8ee00855h
[32] F. Zhou, H. Huang, C. Xiao, S. Zheng, X. Shi, J. Qin, Q. Fu, X. Bao, X. Feng, K. Mullen, Z.S. Wu, *Electrochemically Scalable Production of Fluorine-Modified Graphene for Flexible*

and High-Energy Ionogel-Based Microsupercapacitors, **J. Am. Chem. Soc.**, 140 (2018) 8198-8205, 10.1021/jacs.8b03235
[33] J.Q. Xie, Y.Q. Ji, J.H. Kang, J.L. Sheng, D.S. Mao, X.Z. Fu, R. Sun, C.P. Wong, I*n situ growth of Cu(OH)(2)@FeOOH nanotube arrays on catalytically deposited Cu current collector patterns for high-performance flexible in-plane micro-sized energy storage devices*, **Energy Environ. Sci**., 12 (2019) 194-205, 10.1039/c8ee01979g
[34] C.A. Angell, N. Byrne, J.P. Belieres, *Parallel developments in aprotic and protic ionic liquids: physical chemistry and applications*, **Acc. Chem. Res**., 40 (2007) 1228-1236, 10.1021/ar7001842
[35] M. Anouti, M. Caillon-Caravanier, Y. Dridi, H. Galiano, D. Lemordant, *Synthesis and characterization of new pyrrolidinium based protic ionic liquids. Good and superionic liquids*, **J. Phys. Chem. B**, 112 (2008) 13335-13343, 10.1021/jp805992b
[36] L. Mayrand-Provencher, D. Rochefort, *Influence of the Conductivity and Viscosity of Protic Ionic Liquids Electrolytes on the Pseudocapacitance of RuO_2 Electrodes*, **J. Phys. Chem. C**, 113 (2009) 1632-1639, 10.1021/jp8084149
[37] T. Vogl, P. Goodrich, J. Jacquemin, S. Passerini, A. Balducci, *The Influence of Cation Structure on the Chemical–Physical Properties of Protic Ionic Liquids*, **J. Phys. Chem. C**, 120 (2016) 8525-8533, 10.1021/acs.jpcc.6b01945
[38] L. Mayrand-Provencher, S.X. Lin, D. Lazzerini, D. Rochefort, *Pyridinium-based protic ionic liquids as electrolytes for RuO_2 electrochemical capacitors*, **J. Power Sources**, 195 (2010) 5114-5121, 10.1016/j.jpowsour.2010.02.073
[39] L. Timperman, P. Skowron, A. Boisset, H. Galiano, D. Lemordant, E. Frackowiak, F. Beguin, M. Anouti, *Triethylammonium bis(tetrafluoromethylsulfonyl)amide protic ionic liquid as an electrolyte for electrical double-layer capacitors*, **Phys. Chem. Chem. Phys**., 14 (2012) 8199-8207, 10.1039/c2cp40315c
[40] A. Brandt, J. Pires, M. Anouti, A. Balducci, *An investigation about the cycling stability of supercapacitors containing protic ionic liquids as electrolyte components*, **Electrochim. Acta**, 108 (2013) 226-231, 10.1016/j.electacta.2013.06.118
[41] S. Menne, T. Vogl, A. Balducci, *The synthesis and electrochemical characterization of bis(fluorosulfonyl)imide-based protic ionic liquids*, **Chem. Commun.**, 51 (2015) 3656-3659, 10.1039/c4cc09665g
[42] X. Wang, M. Salari, D.-e. Jiang, J. Chapman Varela, B. Anasori, D.J. Wesolowski, S. Dai, M.W. Grinstaff, Y. Gogotsi, *Electrode material–ionic liquid coupling for electrochemical energy storage*, **Nat. Rev. Mater.** 5 (2020) 787-808, 10.1039/c4cc09665g
[43] L. Köps, F.A. Kreth, A. Bothe, A. Balducci, *High voltage electrochemical capacitors operating at elevated temperature based on 1,1-dimethylpyrrolidinium tetrafluoroborate*, **Energy Storage Mater.** 44 (2022) 66-72, 10.1016/j.ensm.2021.10.006
[44] J.P. Belieres, C.A. Angell, *Protic ionic liquids: preparation, characterization, and proton free energy level representation*, **J. Phys. Chem. B**, 111 (2007) 4926-4937, 10.1021/jp067589u
[45] W. Xu, E.I. Cooper, C.A. Angell, *Ionic Liquids: Ion Mobilities, Glass Temperatures, and Fragilities*, **J. Phys. Chem. B**, 107 (2003) 6170-6178, 10.1021/jp0275894

[46] H.A. Elwan, M. Mamlouk, K. Scott, *A review of proton exchange membranes based on protic ionic liquid/polymer blends for polymer electrolyte membrane fuel cells*, **J. Power Sources**, 484 (2021) 229197, 10.1016/j.jpowsour.2020.229197
[47] M. Yoshizawa, W. Xu, C.A. Angell, *Ionic liquids by proton transfer: vapor pressure, conductivity, and the relevance of DeltapKa from aqueous solutions*, **J. Am. Chem. Soc**., 125 (2003) 15411-15419, 10.1021/ja035783d
[48] K.D. Kreuer, M. Hampele, K. Dolde, A. Rabenau, *Proton Transport in Some Heteropolyacidhydrates a Single-Crystal Pfg-Nmr and Conductivity Study*, **Solid State Ionics**, 28 (1988) 589-593, 10.1016/S0167-2738(88)80107-3
[49] R.C.T. Slade, H.A. Pressman, E. Skou, *Ac and Dc Conductivity Studies of Pelletized 12-Tungstophosphoric Acid and 12-Tungstosilicic Acid Hexahydrates*, **Solid State Ionics**, 38 (1990) 207-211, 10.1016/0167-2738(90)90422-N
[50] S.G. Patnaik, J. Shamsudeen Seenath, D. Bourrier, S. Prabhudev, D. Guay, D. Pech, *Porous $RuO_xN_yS_z$ Electrodes for Microsupercapacitors and Microbatteries with Enhanced Areal Performance*, **ACS Energy Lett**., 6 (2020) 131-139, 10.1021/acsenergylett.0c02017
[51] S. Ardizzone, G. Fregonara, S. Trasatti, *"Inner" and "outer" active surface of RuO_2 electrodes*, **Electrochim. Acta**, 35 (1990) 263-267, 10.1016/0013-4686(90)85068-X
[52] P.F.R. Ortega, J.P.C. Trigueiro, G.G. Silva, R.L. Lavall, *Improving supercapacitor capacitance by using a novel gel nanocomposite polymer electrolyte based on nanostructured SiO_2, PVDF and imidazolium ionic liqui*d, **Electrochim. Acta**, 188 (2016) 809-817, 10.1016/j.electacta.2015.12.056
[53] B. Asbani, B. Bounor, K. Robert, C. Douard, L. Athouel, C. Lethien, J. Le Bideau, T. Brousse, *Reflow Soldering-Resistant Solid-State 3D Micro-Supercapacitors Based on Ionogel Electrolyte for Powering the Internet of Things*, **J. Electrochem. Soc.** 167 (2020) 100551, 10.1149/1945-7111/ab9ccc
[54] S. Rajeevan, S. John, S.C. George, P*olyvinylidene fluoride: A multifunctional polymer in supercapacitor applications*, **J. Power Sources**, 504 (2021) 230037, 10.1016/j.jpowsour.2021.230037